Acquiring an analytical solution and performing a comparative sensitivity analysis for flowing Maxwell upper-convected fluid on a horizontal surface

Siamak Hoseinzadeh[a], Ali Sohani[b], Mohammad Hassan Shahverdian[b], Amin Shirkhani[a], Stephan Heyns[a]

[a]Department of Mechanical and Aeronautical Engineering, University of Pretoria, Pretoria, South Africa
[b]Lab of Optimization of Thermal Systems' Installations, Faculty of Mechanical Engineering-Energy Division, K.N. Toosi University of Technology, P.O. Box: 19395-1999, No. 15-19, Pardis St., Mollasadra Ave., Vanak Sq., Tehran 1999 143344, Iran

*Corresponding author.

hoseinzadeh.siamak@gmail.com
hosseinzadeh.siamak@up.ac.za

Highlights

•An excellent agreement between analytical and numerical solutions is seen.
•The more Deborah is, the lower skin friction coefficient is observed.
•Both drag force and hydraulic boundary layer decline when porosity increases.
•Decrease in Deborah and increase in porosity both lead to enhancing heat transfer.

Abstract

The problem of flowing a Maxwell upper-convected fluid on a horizontal surface is considered here in two conditions. One is the condition in which the plate is made of a porous material, and another one when it is not. For each case, the analytical solution is found using a technique called homotopy perturbation method (HPM). The codes developed in Maple software program are employed for this purpose, and the profiles for velocity and temperature are obtained. The provided analytical solution for each condition is validated using the numerical simulation of the boundary value problem (BVP), and then, a comprehensive sensitivity analysis is carried out. According to the results, for each case, an excellent agreement between the numerical simulation and analytical solution is seen. Moreover, it is found that the skin friction coefficient has a downward trend for both conditions when Deborah goes up. Furthermore, increasing the porosity coefficient is accompanied by decrease in both drag force and hydraulic boundary layer. In addition, for the investigated conditions, having a higher porosity factor leads to an enhancement in the heat transfer, whereas a decrease in Deborah has the same effect.

Keywords: Computer simulation; Horizontal plate; Mathematical solution; Maxwell upper-convected fluid; Porous media; Sensitivity analysis

Nomenclature

Nomenclature

Symbols

c_p	Isobaric heat capacity ($J.kg^{-1}.K^{-1}$)
d	Cutting rate
$\frac{D}{Dt}$	Material derivative
Da	Darcy number (–)
De	Deborah number (–)
f	Function
F	Force (N)
i	Index
j	Index
k	Thermal conductivity ($W.m^{-1}.K^{-1}$)
k*	porosity
L	Velocity gradient tensor
N	Difference between normal stress values (Pa)
p	Auxiliary term
P	Pressure (Pa)
Pr	Prandtl number (–)
Re	Reynolds number (–)
T	Temperature (°C)
u	Velocity ($m.s^{-1}$)
U	Velocity of the free stream ($m.s^{-1}$)
t	Time (s)
x	x direction
y	y direction

Greek symbols

θ	Dimensionless temperature (–)
ρ	Density ($kg.m^{-3}$)
τ	Shear stress (Pa)
δ	Thickness (m)
Δ	Difference
λ	Relaxation time (s)
ψ	Stream function
ν	Kinematic viscosity ($m^2.s^{-1}$)
η	The similarity variable or viscosity factor
φ	Porosity ratio (–)
∂	Partial deriative
ζ	Auxiliary operator

Scripts

c	Relaxation
f	Fluid
m	Mixture
p	Investigated time period
V	Volumetric
s	Solid
w	Wall

Abbreviations

HPM	Homotopy perturbation method
SSSF	Steady state steady flow

1. Introduction

Porous media are being extensively utilized in a wide range of applications from enhancing the performance of power generation units to controlling the temperature of electronic circuits, healthcare products, and so on [1], [2], [3], [4]. Such a great popularity has been the trigger for many investigations in the field [5], [6], [7], and among different topics, modeling the performance has been taken into account as one of the hottest subjects in the area [8], [9], [10]. A model is able to predict the performance of the system for any condition of the effective input parameters [11], [12], [13]. Numerical simulation and analytical solution are two main widely-used ways for modeling [14].

Numerical solution is done when the problem is complex, and the governing equations could not be solved directly. Because of the complexity of the governing equations, modeling the interaction between fluid flow and a porous medium is usually done using the numerical approaches, and several investigations have been employed numerical simulation for modeling the fluid flow inside or outside porous media. Among different aspects, modeling heat transfer is of great importance since it shares valuable information about the exchange of energy, mass, and momentum due to conduction, convection, and radiation, and helps to know the system more comprehensively [15].

As indicated, there have been a huge number of studies that have utilized numerical approach for prediction of the interaction between fluid flow and porous media. Those studies could be categorized into different groups according to various aspects, including the employed method for numerical simulation, the considered fluid, the geometry of porous medium, and the considered effects. Table 1 tries to give a quick summary about the aforementioned criteria of a number of the most related recent studies.

One the other hand, analytical solution could make a bridge to find the value of an output based on the effective input parameters as a function, and could be used as a robust tool for sensitivity analysis and code validation. In addition, compared to the numerical simulation, using an

Table 1. A quick summary of the employed methods, the considered fluids, and the geometries of porous medium in the recent relevant investigations which provided a numerical simulation for interaction of a fluid and a porous medium.

Study	Year	The employed method for numerical simulation	The fluid	The geometry of porous medium	The considered effects
Sheikholeslami [16]	2017	Gauss–Seidel method	Fe_3O_4 nanofluid-water	A curved cavity which has a hot wall on the left	Heat transfer
Toosi and Siavashi [17]	2017	A CFD code based on the reference [18], which utilized finite-volume methodology	Cu particles in water	A square cavity partially in which there was porous medium	Heat transfer
Abdelfatah et al. [19]	2017	Finite difference method	A nano fluid	A core plug	The characteristic of porous media, including permeability
Jourabian et al. [20]	2018	Lattice Boltzmann method	Melting ice as a phase change material	A flat rectangular cavity which has two vertical arranged cylinders	Heat transfer
Khayyer et al. [21]	2018	Lagrangian method	Water	A wave channel with porous media whose porosity was variable	Hydrodynamical characteristics
Ellahi et al. [22]	2019	BVPh 2.0 toolbox in Mathematica	Al_2O_3 nanofluid-water	Two wavy parallel walls	Velocity profile as well as electromagnetic parameters
Su et al. [23]	2019	Discrete element method	Two-phase fluid-particle	A cylinder	Pressure difference in addition to the position of particles in the stream
Talebizadeh Sardari et al. [24]	2020	Combination of enthalpy-porosity and thermal non-equilibrium approaches	A phase change material	A rectangular medium with PCM embedded in a foam that is composed of copper	Heat transfer
Nazari et al. [25]	2020	SIMPLER approach	Al_2O_3 nanofluid-water	A square cavity with two horizontal adiabatic walls	Heat transfer
Omirbekov et al. [26]	2020	Volume-averaging method	Alpha-olefin sulfonate	Foam in porous media	Hydraulic performance
Chen et al. [27]	2020	Least-squares method	Aqueous solution of $BaSO_4$	A reservoir and injection slot	Permeability criteria
Hu et al. [28]	2020	Finite volume CFD method	A Newtonian fluid	Heat exchanger in turbine engine	Heat transfer
Aminian et al. [29]	2020	Finite volume CFD method using ANSYS-FLUENT software program	Al_2O3 and CuO nanofluid- water	A cylinder	Magnetic characteristics as well as heat transfer
Hosseini et al. [30]	2020	Finite element method (X-FEM)	A single-phase fluid	A fracture	Transport phenomena
Massarotti et al. [31]	2020	Characteristic-Based-Split method	Free fluid	A cavity inside a rectangular shape	Heat transfer
Feng et al. [32]	2020	Cascaded lattice Boltzmann method	A mixed convection flow	Cavity in a porous channel	Heat transfer

analytical solution needs a much lower computation time and cost [33]. Therefore, some studies tried to deal with the complexity of problems in the field and provide analytical solutions for them using some “techniques” [34], [35], [36], [37], [38], [39], [40].

Having the similar fashion as the studies which have used numerical simulation, Table 2 is provided to share information about the investigations which have given analytical solutions for interaction of a fluid and a porous medium in different problems. For example, as some of the quite similar items to this study, the research works done by Shao et al. [41], Fahs et al. [42], and Shao et al. [43] could be given as the examples. Shao et al. [41] took the advantage of a method called Fourier–Galerkin approach to find an analytical solution for heat transfer in heterogeneous porous medium, which could be used as a benchmark reference. Moreover, by applying the same technique, i.e., Fourier–Galerkin approach, Fahs et al. [42] proposed an accurate analytical solution for natural convection in a porous enclosure, and employed the solution to investigate the impact of thermal dispersion on that. Additionally, Fourier–Galerkin approach was employed in the study of Shao et al. [43] to present an analytical solution for Darcy-Brinkman double-diffusive convection heat transfer in a geometry, which was a confined saturated porous medium.

Table 2 shows that homotopy perturbation method, also known as HPM, has been utilized in few works to provide analytical solutions. HPM was originally introduced by He [51] and has been used to find the analytical solution for a number of problems in different fields of science [52], [53], [54], [55], [56]. However, it has not been employed for the problem of flowing a Maxwell upper-convected fluid on a flat porous plate. Moreover, a comparative study to find the impact of changing the effective parameters on the heat transfer of this fluid has not been carried out yet. The explained issues could be considered as the gap of the research. In another word, to the best of authors' knowledge and based on the conducted literature review, all previous studies have neglected to provide an analytical solution for flowing the Maxwell upper-convicted fluid on a porous medium fluid perform the sensitivity analysis to find the impact of effective parameters. In fact, they have focused on the fluids with simpler physics, like the Newtonian ones.

Despite progress in numerical model development, analytical solutions are still important as they provide direct relation between model output and input parameters (so they are helpful in performing sensitivity analysis) and they are of first importance for code validation. The results presented in this paper (especially, the comparison between analytical and numerical solutions) can serve as data for code verification and benchmarking. Therefore, providing the analytical solution for flowing the Maxwell upper-convected fluid using HPM method, and comparing the obtained solution with the condition in which the plate is not porous could be taken into account as the novelties of the paper.

2. Methodology

2.1. Problem definition

As previously mentioned, the goal of this investigation is to solve the governing equations for flowing Maxwell upper-convected fluid on a horizontal surface in two conditions. One is the condition in which the plate is made of a porous medium, and another is the horizontal surface whose material is not porous. The goal is achieved by employing HPM, as described in the rest of this part, and by obtaining the distribution for temperature (

Table 2. A quick summary of the recent relevant investigations carried out for providing an analytical solution for interaction of a fluid and a porous medium.

Study	Year	The employed method to prepare the analytical solution	The fluid	The geometry of porous medium	The considered effects
Shao et al. [41]	2015	Fourier–Galerkin approach	A fluid which had Darcy-Brinkman heat, flow, and mass transfer	A square cavity	Heat transfer
Shao et al. [43]	2016	Fourier–Galerkin approach	A fluid with double-diffusive convection	A square cavity	Heat transfer
Obembe et al. [44]	2017	Modification of the memory-based approach	Slightly compressible fluid	Fractal	Hydraulic performance
Shirkhani et al. [45]	2018	Homotopy perturbation method	Newtonian fluid	Two parallel discs	
Nakshatrala et al. [46]	2018	Green's function method	A single-phase fluid which was incompressible	A rigid medium which featured double porosity	Mass transfer and velocity profile
Joodat et al. [47]	2018	mechanics-based solution verification	An incompressible fluid	Hollow sphere	Mass transfer and velocity profile
Fahs et al. [42]	2019	Fourier–Galerkin approach	A fluid with internal natural convection	A square type of cavity which has the slip velocity boundary	Heat transfer
Hoseinzadeh et al. [48]	2019	Homotopy perturbation method	A single-phase fluid	A fin whose cross section was rectangular	Heat transfer
Nabizadeh et al. [49]	2020	Using separation variable	Spherical fluid	A reservoir	Hydraulic characteristics, including the dimensionless pressure
Ghanbari Ashrafi et al. [50]	2020	Homotopy perturbation method	Newtonian fluid	A flat plate	Heat transfer, as well as velocity and stress profiles

) and velocity (u). These two parameters are determined while they are dependent on x and y, as the independent parameters. Fig. 1 shows the schematic design of the problem.

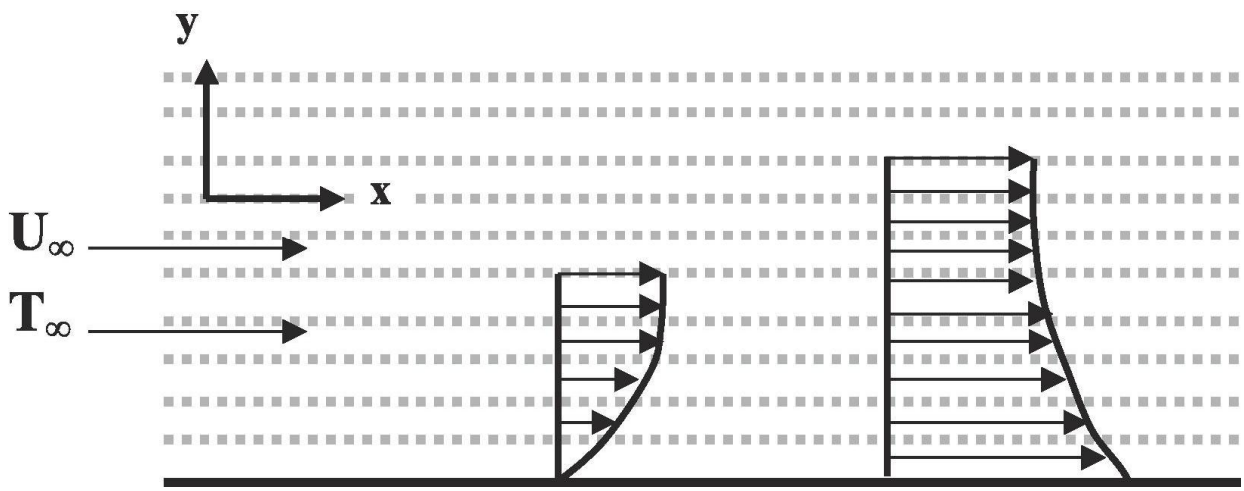

Fig. 1. The Schematic statement of the problem.

Maxwell material refers to a substance which is viscous and elastic at the same time, and in fluid mechanics, upper-convected model represents the behavior of a Maxwell material when large deformations take place. In such case, upper-convected time derivative is employed for modeling, and the name “upper-convected” comes from that [57].

Additionally, for developing the analytical solution, the continuity is assumed for the medium while the fluid is considered incompressible. Not changing the properties and working in steady state steady flow (SSSF) condition are two other assumptions for the investigation. Moreover, no phase change process takes place in the system and all the solid particles are thought to have the same specifications, including the shape.

2.2. Governing equations

Continuity, momentum, and energy equations are taken into account as the three main types of governing equations for the investigated system. Considering the point that, based on the assumptions, no changes in properties happens, the momentum equation could be solved separate from the energy equation.

When the flow is laminar and there is SSSF condition, the governing continuity and momentum equations are:

$$\frac{\partial u}{\partial x} + \frac{\partial \vartheta}{\partial y} = 0 \tag{1}$$

$$\rho\left(u\frac{\partial u}{\partial x} + \vartheta\frac{\partial u}{\partial y}\right) = -\frac{\partial p}{\partial x} + \frac{\partial \tau_{xx}}{\partial x} + \frac{\partial \tau_{xy}}{\partial y} + F_V \tag{2}$$

$$\rho\left(u\frac{\partial v}{\partial x} + \vartheta\frac{\partial v}{\partial y}\right) = -\frac{\partial p}{\partial y} + \frac{\partial \tau_{yx}}{\partial x} + \frac{\partial \tau_{yy}}{\partial y} + F_V \tag{3}$$

In which ρ is shows density while $\frac{\partial \tau_{yy}}{\partial y}$ and $\frac{\partial \tau_{xx}}{\partial x}$, and $\frac{\partial \tau_{yx}}{\partial y}$ and $\frac{\partial \tau_{xy}}{\partial x}$ are the elastic and viscosity terms, respectively. F_v also stands for volumetric force. According to the boundary layer theory and by employing order of magnitude, the condition reported in Eq. (4) for the investigated problem exists.

$$u = O(1) \quad \vartheta = O(\delta) \quad x = O(1) \quad y = O(\delta) \quad \frac{\tau_{xx}}{\rho} = O(1) \frac{\tau_{xy}}{\rho} = O(\delta) \frac{\tau_{yy}}{\rho} = O(\delta^2) \tag{4}$$

Through making Eqs. (2), (3) simple, Eqs. (5), (6) are achieved:

$$\rho\left(u\frac{\partial u}{\partial x} + \vartheta\frac{\partial u}{\partial y}\right) = -\frac{dp}{dx} + \frac{\partial \tau_{xx}}{\partial x} + \frac{\partial \tau_{xy}}{\partial y} - \frac{\mu}{k}u \tag{5}$$

$$\frac{\partial P}{\partial y} = 0 \tag{6}$$

where $\frac{\mu}{k}u$ and k show Darcy term and penetration factor, respectively. In case the medium is not porous, the pressure changes in x direction could be neglected. If not, the genral form of Darcy approach can be utilized.

$$\rho\left(u\frac{\partial u}{\partial x} + \vartheta\frac{\partial u}{\partial y}\right) = -\frac{dp}{dx} + \frac{\partial \tau_{xx}}{\partial x} + \frac{\partial \tau_{xy}}{\partial y} - \frac{\mu}{k}u \tag{7}$$

$$\frac{\partial u}{\partial x} + \frac{\partial \vartheta}{\partial y} = 0 \tag{8}$$

In Eqs. (7), (8), five unknown variables could be identified, which are: P, τ_{xy}, τ_{xx}, ϑ , and u.

A system of equations could be solved when number of equations are equal to number of unknown variables. Therefore, three more (auxiliary) equations are needed. The first auxiliary equation could be written based on the properties of the Maxwell fluid, which indicates that the tensors for tension and changes rate are related together based on Eq. (9):

$$\tau_{ij} + \lambda\frac{\Delta}{\Delta t}\tau_{ij} = 2\eta d_{ij} \tag{9}$$

η , λ, and $\frac{\Delta}{\Delta t}$ denote the viscosity factor, time of relaxation, and the derivative of time, respectively. Eq. (10) could be applied for calculation of the term $\frac{\Delta}{\Delta t}\tau_{ij}$:

$$\frac{\Delta \tau_{ij}}{\Delta t} = \frac{D\tau_{ij}}{Dt} - L_{jk}\tau_{ik} - L_{ik}\tau_{kj} \tag{10}$$

All the used terms in Eq. (10) have been introduced previously except for L_{ij}. This is the tensor for velocity gradient.

Putting all the terms from the introduced equations into Eq. (7) results in achieving Eq. (11) as the momentum equation for the Maxwell fluid:

$$u\frac{\partial u}{\partial x} + \vartheta\frac{\partial u}{\partial y} + \lambda\left[u^2\left(\frac{\partial^2 u}{\partial x^2}\right) + \vartheta^2\left(\frac{\partial^2 u}{\partial y^2}\right) + 2u\vartheta\left(\frac{\partial^2 u}{\partial x \partial y}\right)\right] = -\frac{dp}{dx} + \nu\left(\frac{\partial^2 u}{\partial y^2}\right) - \frac{\nu}{k}u \tag{11}$$

Based on the considered assumptions and due to the constant rate of free flow:

$$\frac{dp}{dx} = -\frac{\mu}{K}U \tag{12}$$

Consequently, as the final equation, Eq. (13) is obtained:

$$u\frac{\partial u}{\partial x} + \vartheta\frac{\partial u}{\partial y} + \lambda\left[u^2\left(\frac{\partial^2 u}{\partial x^2}\right) + \vartheta^2\left(\frac{\partial^2 u}{\partial y^2}\right) + 2u\vartheta\left(\frac{\partial^2 u}{\partial x \partial y}\right)\right] = \nu\left(\frac{\partial^2 u}{\partial y^2}\right) - \frac{\nu}{k}(u - U) \tag{13}$$

Since there is no slip, the boundary conditions indicated in Eq. (14) are imposed to the problem:

$$aty = 0;\ \ u = 0;\ \ \vartheta = 0aty \to \infty;\ \ u \to U \tag{14}$$

For energy equation, since the problem is solved for SSSF conditions in which the changes in properties, including the temperature are zero and no heat generation takes place, Eqs. (15), (16) could be written:

$$u\frac{\partial T}{\partial x} + \vartheta\frac{\partial T}{\partial y} = \frac{k_m}{(\rho c_p)_f}\left(\frac{\partial^2 T}{\partial y^2}\right) \tag{15}$$

$$k_m = (1 - \varphi)k_s + \varphi k_f \tag{16}$$

In Eqs. (15), (16) the conductivity of solid parts and fluid are indicated by k_s and $k_{f,}$, respectively. Moreover, $\frac{k_m}{(\rho c_p)_f}$ is defined as that is called the thermal distribution. Additionally, the corresponding boundary condition is:

$$aty = 0;\ \ T = T_w \text{ at } y \to \infty;\ \ T \to T_\infty \tag{17}$$

2.3. Transforming equations to ordinary format

Stream function is defined based on Eq. (18):

By defining the flow function, we can reduce the number of unknowns in the Eq. (13) to one.

$$u = \frac{\partial \psi}{\partial y}\ \ \vartheta = -\frac{\partial \psi}{\partial x} \tag{18}$$

If Eq. (21) is considered, Eq. (15) could be stated in the form of Eq. (22):

$$\left(\frac{\partial \psi}{\partial y}\right)\left(\frac{\partial^2 \psi}{\partial x \partial y}\right) - \left(\frac{\partial \psi}{\partial x}\right)\left(\frac{\partial^2 \psi}{\partial y^2}\right) + \lambda\left[\left(\frac{\partial \psi}{\partial y}\right)^2\left(\frac{\partial^3 \psi}{\partial y \partial x^2}\right)\right.$$
$$\left. + \left(\left(\frac{\partial \psi}{\partial x}\right)^2\left(\frac{\partial^3 \psi}{\partial y^3}\right) - 2\left(\frac{\partial \psi}{\partial y}\right)\left(\frac{\partial \psi}{\partial x}\right)\left(\frac{\partial^3 \psi}{\partial x \partial y^2}\right)\right)\right] = \nu\left(\frac{\partial^3 \psi}{\partial y^3}\right) - \frac{\nu}{k}\left(\frac{\partial \psi}{\partial y} - U\right) \tag{19}$$

The similarity variable is defined as $\eta = y\sqrt{\frac{U}{\nu x}}$. Then:

$$\frac{u}{U} = f'(\eta) \Rightarrow Uf'(\eta) = \frac{\partial \psi}{\partial y} \Rightarrow Uf'(\eta) = \frac{\partial \psi}{\partial \eta}\frac{\partial \eta}{\partial y} \Rightarrow Uf'(\eta)$$
$$= \sqrt{\frac{U}{\vartheta x}}\frac{\partial \psi}{\partial \eta} \Rightarrow \sqrt{U\vartheta x}f'(\eta)d\eta = d\psi\psi = \sqrt{U\vartheta x}f(\eta) \quad (20)$$

After taking advantage of simplifications, Eq. (21) is achieved:

$$-2U^2kxf''(\eta)f(\eta)+U^3k\lambda\eta f'^2(\eta)f''(\eta)+U^3k\lambda f'''(\eta)f^2(\eta)+2U^3k\lambda f'(\eta)f(\eta)f''(\eta)$$
$$-4xU^2kf'''(\eta)+4x^2U\nu f'(\eta)-4Ux^2\nu = 0 \quad (21)$$

When both sides of Eq. (21) are divided by k', Eq. (22) is obtained:4

$$-2U^2xf''(\eta)f(\eta)+U^3\lambda\eta f'^2(\eta)f''(\eta)+U^3\lambda f'''(\eta)f^2(\eta)+2U^3\lambda f'(\eta)f(\eta)f''(\eta)$$
$$-4xU^2f'''(\eta)+4\frac{x^2}{k}U\nu f'(\eta)-4U\frac{x^2}{k}\nu = 0 \quad (22)$$

Darcy number for the direction × could be defined as ($Da_x = \frac{k}{x^2} = \frac{k_0}{x}k = k_0x$). If both sides are multiplied in (−1), and then, they are divided by and since based on the definition of the problem in two-dimensional system (Fig. 1), the penetration is in the × axis:

$$\frac{1}{2}f''(\eta)f(\eta)-\frac{U\lambda}{4x}\eta f'^2(\eta)\ddot{f}(\eta)-\frac{U\lambda}{4x}f'''(\eta)f^2(\eta)-\frac{U\lambda}{2x}f'(\eta)f(\eta)f''(\eta)+f'''(\eta)$$
$$-\frac{1}{Da_x}\frac{\nu}{Ux}f'(\eta)+\frac{1}{Da_x}\frac{\nu}{Ux} = 0 \quad (23)$$

Therefore:

$$f'''(\eta)+\frac{1}{2}f(\eta)f''(\eta)-\frac{\lambda U}{4x}\left(2f(\eta)f'(\eta)f''(\eta)+f^2(\eta)f'''(\eta)+\eta f'^2(\eta)f''(\eta)\right)$$
$$-\frac{1}{Da_xRe_x}(f'(\eta)-1) = 0 \quad (24)$$

The term $\frac{\lambda U}{4x}$ is defined as Deborah number (De) while $k^* = \frac{1}{Da*Re}$. Consequently, Eq. (27) changes to Eq. (28) and the corresponding boundary condition is written based on Eq. (29):

$$f'''(\eta)+\frac{1}{2}f(\eta)f''(\eta)-De\left(2f(\eta)f'(\eta)f''(\eta)+f^2(\eta)f'''(\eta)+\eta f'^2(\eta)f''(\eta)\right)-k^*(f'(\eta)-1)$$
$$= 0 \quad (25)$$

$$\eta = 0;\ f(\eta) = 0\ f'(\eta) = 0\eta \to \infty;\ f'(\eta) \to 1 \quad (26)$$

In addition, by defining the dimensionless temperature in the form of ($\theta = \frac{T-T_\infty}{T_w-T_\infty}$), Eq. (27) is achieved:

$$\theta'(\eta)\sqrt{\frac{U}{\nu x}}f(\eta)\nu^2\rho_f c_{pf}x + 2k_m\theta''(\eta)\sqrt{\nu xU} = 0 \quad (27)$$

If two sides of Eq. (27) is divided by $\sqrt{\frac{U}{\nu x}}$, Eq. (28) is obtained:

$$\theta'(\eta)f(\eta)\nu^2\rho_f c_{pf}x + 2k_m\nu x\theta''(\eta) = 0 \tag{28}$$

Eq. (28) could be divided by $2k_m\nu x$, which leads to writing Eq. (29):

$$\frac{\nu\rho_f c_{pf}}{2k_m}\theta'(\eta)f(\eta) + \theta''(\eta) = 0 \tag{29}$$

Consequently:

$$\theta''(\eta) + \frac{1}{2}\Pr.f(\eta)\theta'(\eta) = 0 \tag{30}$$

Boundary conditions are also stated as Eq. (31) shows:

$$\eta = 0;\ \ \theta(\eta) = 0\eta \to \infty;\ \ \theta(\eta) \to 1 \tag{31}$$

In this study, in addition to evaluation of the accuracy of solution for the two aforementioned conditions, the effect of changes in the viscoelastic parameter (De) and the penetration coefficient (k*) on the velocity profile and fluid temperature will be also investigated for them. Checking the accuracy is done by comparing the results of HPM with the boundary value problem (BVP) method.

It is also worth mentioning that Maple software has some libraries, containing written codes, to solve boundary value problem (BVP), and in this study, numerical solution was found by employing that. More details about the commands and the working principle of the libraries are available in [58].

2.4. More detailed equations for the two cases

2.4.1. Case I: The Maxwell upper-convected fluid on the horizontal surface

For this case, k* = 0. As a result:

$$f'''(\eta) + \frac{1}{2}f(\eta)f''(\eta) - De\left(2f(\eta)f'(\eta)f''(\eta) + f^2(\eta)f'''(\eta) + \eta f^{'2}(\eta)f''(\eta)\right) = 0 \tag{32}$$

$$\eta = 0;\ \ f(\eta) = 0\ \ f'(\eta) = 0\eta \to \infty;\ \ f'(\eta) \to 1 \tag{33}$$

In order to obtain $f(\eta)$, an auxiliary linear operator shown in Eq. (34) is chosen:

$$L(u) = f'''(\eta) + \zeta f''(\eta) \tag{34}$$

It results in obtaining the differential equations indicated in Eqs. (35), (36):

$$\frac{d^3f}{d\eta^3} + \zeta \frac{d^2f}{d\eta^2} = 0 \tag{35}$$

$$f(0) = 0 \quad f'(0) = 0 \quad f'(\infty) = 1 \tag{36}$$

The value of ζ is determined based on the considered constant parameters for the problem and adjusting the values with the numerical solution in a way that the highest accuracy is achieved. For example, when De = 0.01, the condition with $\zeta = 1.3$ has the highest accuracy with numerical solution as shown in Fig. 2.

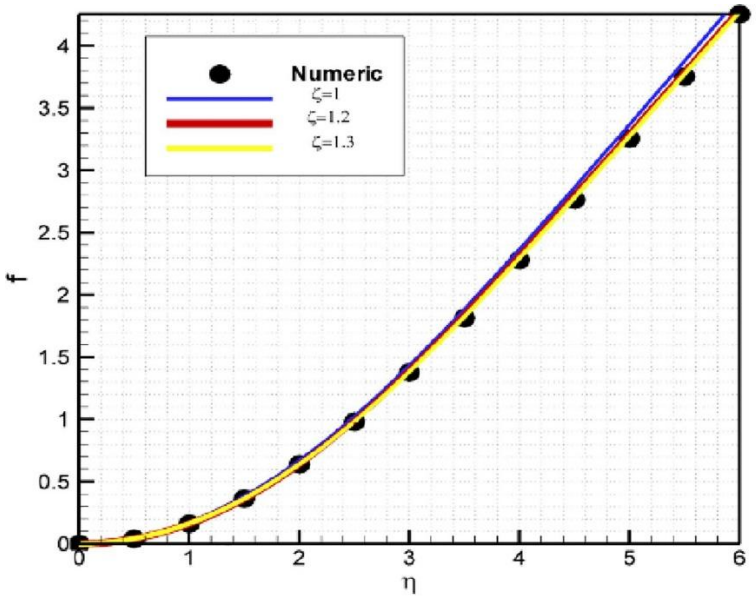

(a)

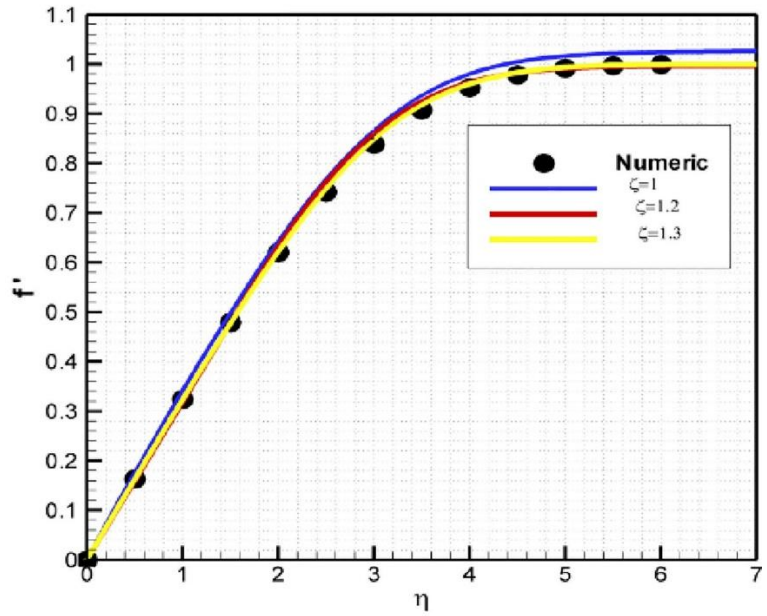

(b)

Fig. 2. The process of finding the best value of ζ for $k^* = 0, De = 0.01$ in case I a) the diagram of f, i.e., the stream function, b) the diagram of f', i.e., velocity distribution.

The differential equation could be solved in combination with the linear auxiliary operator, which leads to obtaining Eq. (37):

$$f^0(\eta) = -\frac{10}{13} + \eta + \frac{10}{13}e^{(-\frac{13}{10}\eta)} \tag{37}$$

Based on HPM working principle, Eqs. (38), (39) could be written:

$$(1-p)L\left[F(\eta;p) - f^0(\eta)\right] + p\left[L\{F(\eta;p) + N\{F(\eta;p)\}\right] = 0 \tag{38}$$

$$F(0;p) = 0 \quad F'^{(0;p)} = 0 \quad F'(\infty;p) = 1 \tag{39}$$

Where p is called the embedding parameter; it is in the range of $p \in [0 \text{ and } 1]$. As a result:

$$F(\eta;0) = f_0(\eta) \quad F(\eta;1) = f(\eta) \tag{40}$$

According to the definition and considered values, when p increases from zero to one, $F(\eta;p)$ changes from $f_0(\eta)$ to $f(\eta)$. In case $k^* = 0$ and De = 0.01:

$$\begin{aligned}&(1-p)\left(f'''(\eta) + 1.1f''(\eta) - \left(-\frac{10}{13} + \eta + \frac{10}{13}e^{(-\frac{13}{10}\eta)}\right)\right)\\&+p\left(f''' + \frac{1}{2}f(\eta)f'' - 0.02f(\eta)f'(\eta)f'' + 0.01f^2(\eta)f'''' + 0.01\eta f'^2(\eta)f''(\eta)\right)\\&= 0\end{aligned} \tag{41}$$

By substituting $f(\eta) = f_0(\eta) + pf_1(\eta) + \cdots + p^6 f_6(\eta)$ and arranging Eq. (41) based on p, the coefficients for p^0, p^1,... and p^6, and after that $f_0(\eta)$, $f_1(\eta)$, ... and $f_6(\eta)$ are obtained. Finally, $f(\eta)$ is also computed through adding $f_0(\eta)$, $f_1(\eta)$, ..., and $f_6(\eta)$.

$$\begin{aligned}f(\eta) = &-0.9091060 + 1.0000016\eta + 0.9091060e^{-1.10000\eta} + 0.1300336e^{-1.10000\eta}\\&+ 0.123973e^{-2.20000\eta}\eta - 0.004591e^{-3.30000\eta}\eta + 0.206620e^{-2.20000\eta}\\&+ 0.00765266e^{-3.30000\eta} - 0.0333350\eta^3e^{-1.10000\eta} - 0.181823\eta^2e^{-1.10000\eta}\\&+ 0.5041365e^{-1.10000\eta}\eta + 0.0000015183\eta^2 - 0.0006624\eta - 0.3443066\\&+ 0.00000000000076\eta^3 + 0.0005833\eta^2 + 0.0104829\eta + 0.63041073e^{-2.20000\eta}\eta\\&+ 0.746989e^{-3.30000\eta}\eta + \cdots + 0.0016075\eta e^{-4.40000\eta} - 0.356333\end{aligned} \tag{42}$$

Having the similar fashion as the way to determine Eq. (42), Eqs. (43) to (49) could be written, and then, $\theta(\eta)$ that could be assumed as the summation of three terms of $\theta_0(\eta) + p\theta_1(\eta) + p^2\theta_2(\eta)$ is determined. Eqs. (50) to (52) introduce the obtained $\theta_0(\eta)$, $\theta_1(\eta)$, and $\theta_2(\eta)$, respectively.

$$L(u) = \theta''(\eta) + \theta'(\eta) \tag{43}$$

$$\frac{d^2\theta}{d\eta^2} + \frac{d\theta}{d\eta} = 0 \tag{44}$$

$$\theta(0) = 0, \qquad \theta(\infty) = 1 \tag{45}$$

$$\theta^0(\eta) = 1 - e^{-\eta} \tag{46}$$

$$(1-p)L\left[\theta(\eta;p) - \theta^0(\eta)\right] + p[L\{\theta(\eta;p) + N\{\theta(\eta;p)\}] = 0 \tag{47}$$

$$\theta(0;p) = 0\theta(\infty;p) = 1 \tag{48}$$

$$(1-p)(\theta''(\eta) + \theta'(\eta) - (1-e^{-\eta})) + p\,(\theta''(\eta) + \tfrac{1}{2}0.7f(\eta)\theta'(\eta)) = 0 \tag{49}$$

$$\theta_0(\eta) = 1.000045402 - 1.000045402e^{-\eta} \tag{50}$$

$$\begin{aligned}\theta_1(\eta) = {} & -0.000066\eta^3 e^{-\eta} - 1.21006\eta e^{-\eta} + 0.17670\eta^2 e^{-\eta} - 0.0000512\eta^3 e^{-4.30000\eta} \\ & - 0.001476\eta^5 e^{-2.10000\eta} + 0.0004520\eta^4 e^{-3.20000\eta} - 0.0003285060603\eta e^{-3.40000\eta} \\ & - 0.0001474710324e^{-4.60000\eta} + 0.2745382680e^{-\eta} - 0.0002768\end{aligned} \tag{51}$$

$$\begin{aligned}\theta_2(\eta) & \\ = {} & 0.00000002025\eta^6 e^{-8.70000\eta} - 0.0000000797\eta^5 e^{-8.70000\eta} - 0.000001337\eta^8 e^{-4.30000\eta} \\ & - 0.00000000006969348020\eta^8 e^{-\eta} - 0.0009932741947\eta e^{-4.60000\eta} \\ & - 0.00441469983\eta^5 e^{-2.20000\eta} + 0.0006047123667\eta^6 e^{-2.20000\eta} \\ & + 0.0034736092\eta^3 e^{-3.40000\eta} - \cdots - 0.01533864715\eta^4 e^{-\eta}\end{aligned} \tag{52}$$

2.4.2. Case II: The Maxwell upper-convected fluid flow in the porous medium on the horizontal surface

Based on the defined problem, the equation and corresponding boundary conditions for this case are:

$$f'''(\eta) + \tfrac{1}{2}f(\eta)f''(\eta) - De\left(2f(\eta)f'(\eta)f''(\eta) + f^2(\eta)f'''(\eta) + \eta f^{'2}(\eta)f''(\eta)\right) - k^*(f'(\eta) - 1) = 0 \tag{53}$$

$$\eta = 0;\ \ f(\eta) = 0\ \ f'(\eta) = 0 \eta \to \infty;\ \ f'(\eta) \to 1 \tag{54}$$

By following the similar way as the previous case, an auxiliary parameter is defined:

$$L(u) = f'''(\eta) + \zeta f''(\eta) \tag{55}$$

Which results in obtaining differential equation introduced in Eq. (56):

$$\frac{d^3f}{d\eta^3} + \zeta\frac{d^2f}{d\eta^2} = 0 \tag{56}$$

With the boundary conditions reported in Eq. (57):

$$f(0) = 0\ \ f'(0) = 0\ \ f'(\infty) = 1 \tag{57}$$

Similar to the previous case, here, finding the best value for ζ is done from the graphic way. For example, for the investigated case, when k* = 0.2 and De = 0.1, $\zeta = 1.2$ has the highest accuracy with the numerical solution, as shown in Fig. 3.

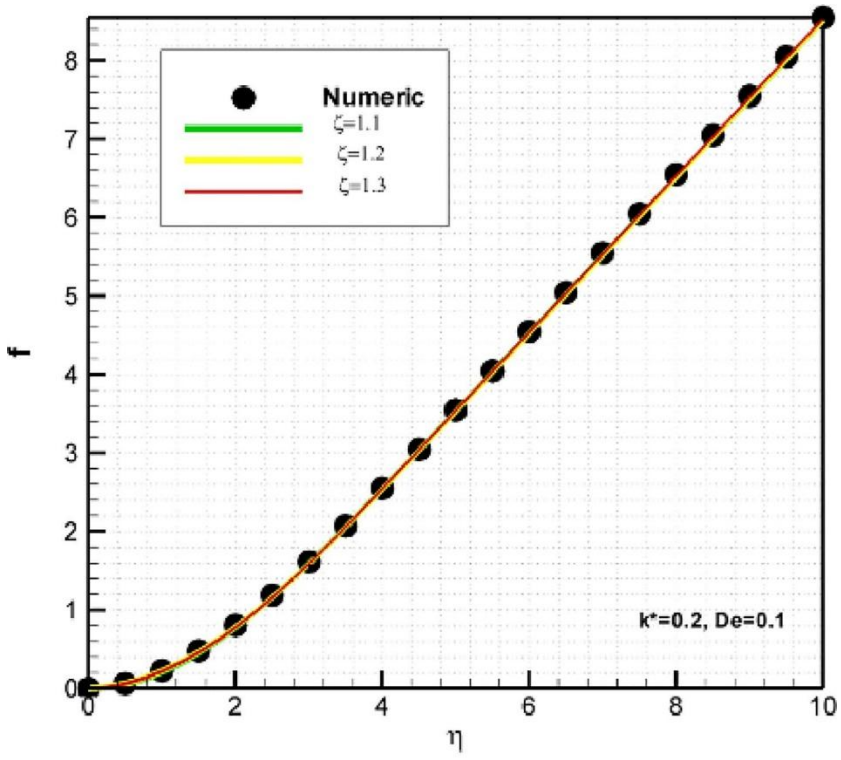

(a)

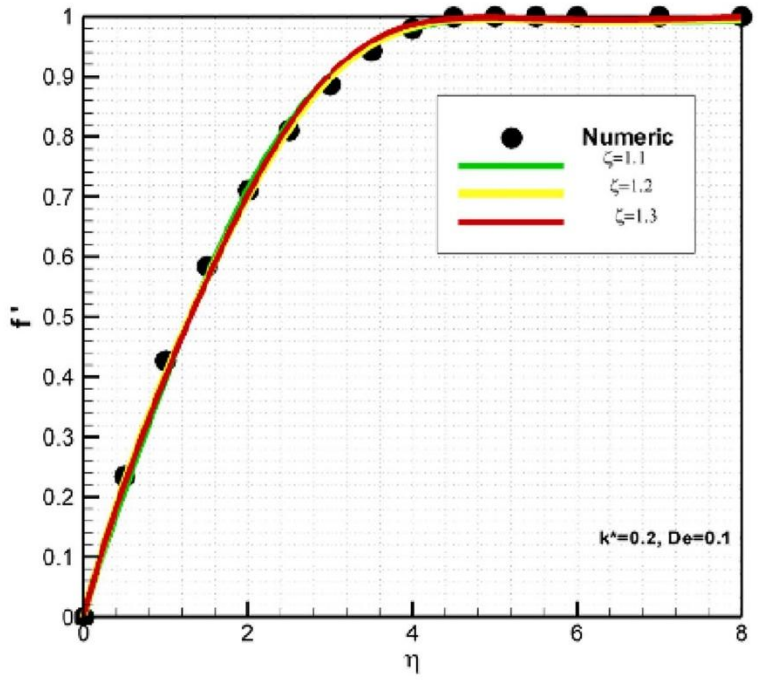

(b)

Fig. 3. The process of finding the best value of ζ for $k^* = 0.2, De = 0.1$ in case II a) the diagram of f, i.e., the stream function, b) the diagram of f', i.e., velocity distribution.

The guess function for the investigated differential equations is:

$$f^0(\eta) = -\frac{10}{12} + \eta + \frac{10}{12}e^{\left(-\frac{12}{10}\eta\right)} \quad (58)$$

By applying HPM, the analytical solution for the function f could be obtained. The equation for the condition in which $k^* = 0.2$ and $D_e = 0.1$ is:

$$(1-p)\left(f'''(\eta)+1.2f''(\eta)-\left(-\frac{10}{12}+\eta+\frac{10}{12}e^{\left(-\frac{12}{10}\eta\right)}\right)\right)$$
$$+p\left(f'''(\eta)+\frac{1}{2}f(\eta)f''(\eta)-0.2f(\eta)f'(\eta)f''(\eta)+0.1f^2(\eta)f'''(\eta)+0.1\eta f'^2(\eta)f''(\eta)-0.2f'(\eta)+0.2\right)$$
$$=0 \quad (59)$$

If $f(\eta) = f_0(\eta)+pf_1(\eta)+p^2f_2(\eta)$ and this equation is arranged with respect to *p*, the terms are:

$$f_0(\eta) = -0.9091060 + 1.0000016\eta + 0.9091060e^{-1.10000\eta} \quad (60)$$

$$f_1(\eta) = 0.1300336e^{-1.10000\eta} + 0.123973e^{-2.20000\eta}\eta - 0.004591e^{-3.30000\eta}\eta$$
$$+ 0.206620e^{-2.20000\eta} + 0.00765266e^{-3.30000\eta} - 0.0333350\eta^3e^{-1.10000\eta}$$
$$- 0.181823\eta^2e^{-1.10000\eta} + 0.5041365e^{-1.10000\eta}\eta + 0.0000015183\eta^2 - 0.0006624\eta$$
$$- 0.344306 \quad (61)$$

$$f_2(\eta)$$
$$= 0.00000000000076\eta^3 + 0.0005833\eta^2 + 0.0104829\eta + 0.63041073e^{-2.20000\eta}\eta$$
$$+ 0.746989e^{-3.30000\eta}\eta + 0.392826e^{-1.10000\eta} - 0.0364027e^{-1.10000\eta}\eta^3$$
$$+ 0.3579837e^{-1.10000\eta}\eta^2 - 0.262531e^{-1.10000\eta}\eta + 0.0851281e^{-2.200000\eta}$$
$$+ 0.0427267e^{-3.300000\eta} - 0.00552289e^{-4.4000000\eta} + 0.000315603e^{-5.5000000\eta}$$
$$+ 0.0435767e^{-2.20000\eta}\eta^2 + 0.0126068e^{-3.30000\eta}\eta^2 - 0.004848e^{-1.10000\eta}\eta^4$$
$$- 0.0523448e^{-2.20000\eta}\eta^3 + 0.009948e^{-3.30000\eta}\eta^3 + 0.0046669e^{-1.10000\eta}\eta^5$$
$$- 0.009091e^{-2.20000\eta}\eta^4 + 0.005059e^{-3.30000\eta}\eta^4 + 0.0016075\eta e^{-4.40000\eta} - 0.356333 \quad (62)$$

$f(\eta)$ is obtained when three equations are added together:

$$f(\eta) = -0.9091060 + 1.0000016\eta + 0.9091060e^{-1.10000\eta} + 0.1300336e^{-1.10000\eta}$$
$$+ 0.123973e^{-2.20000\eta}\eta - 0.004591e^{-3.30000\eta}\eta + 0.206620e^{-2.20000\eta}$$
$$+ 0.00765266e^{-3.30000\eta} - 0.0333350\eta^3e^{-1.10000\eta} - 0.181823\eta^2e^{-1.10000\eta}$$
$$+ 0.5041365e^{-1.10000\eta}\eta + 0.0000015183\eta^2 - 0.0006624\eta - 0.3443066$$
$$+ 0.00000000000076\eta^3 + 0.0005833\eta^2 + 0.0104829\eta + 0.63041073e^{-2.20000\eta}\eta$$
$$+ 0.746989e^{-3.30000\eta}\eta + 0.392826e^{-1.10000\eta} - 0.0364027e^{-1.10000\eta}\eta^3$$
$$+ 0.3579837e^{-1.10000\eta}\eta^2 - 0.262531e^{-1.10000\eta}\eta + 0.0851281e^{-2.200000\eta}$$
$$+ 0.0427267e^{-3.300000\eta} - 0.00552289e^{-4.4000000\eta} + 0.000315603e^{-5.5000000\eta}$$
$$+ 0.0435767e^{-2.20000\eta}\eta^2 + 0.0126068e^{-3.30000\eta}\eta^2 - 0.004848e^{-1.10000\eta}\eta^4$$
$$- 0.0523448e^{-2.20000\eta}\eta^3 + 0.009948e^{-3.30000\eta}\eta^3 + 0.0046669e^{-1.10000\eta}\eta^5$$
$$- 0.009091e^{-2.20000\eta}\eta^4 + 0.005059e^{-3.30000\eta}\eta^4 + 0.0016075\eta e^{-4.40000\eta} - 0.356333 \quad (63)$$

Having obtained $f(\eta)$, $\theta(\eta)$, which is considered in the form of $\theta(\eta)= \theta_0(\eta)+p\theta_1(\eta)+p^2\theta_2(\eta)$ could be also obtained. Eqs. (63), (64), (65) introduce $\theta_0(\eta), \theta_1(\eta)$, and $\theta_2(\eta)$, respectively.

$$\theta_0(\eta)= 1.000045402 - 1.000045402e^{-\eta} \tag{64}$$

$$\begin{aligned}\theta_1(\eta)= &-0.000066\eta^3e^{-\eta} - 1.21006\eta e^{-\eta} + 0.17670\eta^2e^{-\eta} - 0.0000512\eta^3e^{-4.30000\eta}\\ &- 0.001476\eta^5e^{-2.10000\eta} + 0.0004520\eta^4e^{-3.20000\eta} - 0.0003285060603\eta e^{-3.40000\eta}\\ &- 0.0001474710324e^{-4.60000\eta} + 0.2745382680e^{-\eta} - 0.0002768\end{aligned} \tag{65}$$

$$\begin{aligned}&\theta_2(\eta)\\ &= 0.00000002025\eta^6e^{-8.70000\eta} - 0.0000000797\eta^5e^{-8.70000\eta}\\ &- 0.000001337\eta^8e^{-4.30000\eta} - 0.00000000006969348020\eta^8e^{-\eta}\\ &- 0.0009932741947\eta e^{-4.60000\eta} - 0.00441469983\eta^5e^{-2.20000\eta}\\ &+ 0.0006047123667\eta^6e^{-2.20000\eta} + 0.0034736092\eta^3e^{-3.40000\eta} -\\ &\cdots - 0.01533864715\eta^4e^{-\eta}\end{aligned} \tag{66}$$

3. Results and discussion

As the name also indicates, the results of this work will be presented in this part.

3.1. Validation of the proposed analytical solution by HPM

This part shares the information about validation of the developed analytical solution. Validation is done by taking advantage of the numerical solution found based on BVP in Maple software.

3.1.1. Case I: The Maxwell upper-convected fluid on the horizontal surface

As mentioned before, checking the accuracy of the proposed analytical solution by HPM is done using the numerical solution. For this purpose, the estimation of four important performance parameters, namely stream function, as well the distribution of velocity, stress, and dimensionless temperature are compared together. The results are given in Fig. 4, where an excellent agreement between the prediction of HPM and numerical simulation is observed. Therefore, the analytical solution which is provided by HPM has been validated, and it could be utilized for further analyses, including sensitivity analysis.

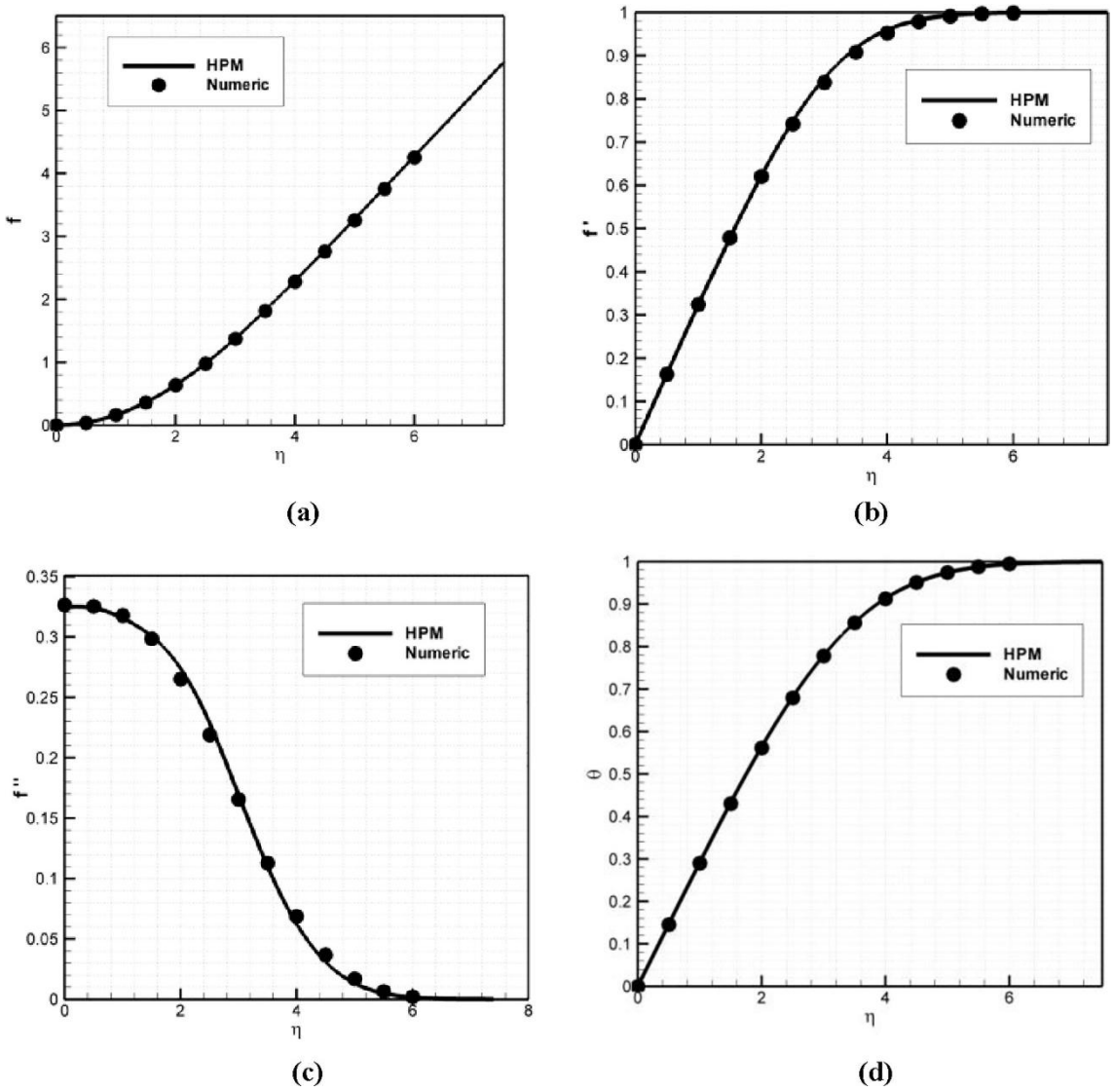

Fig. 4. Checking the prediction ability of the proposed analytical solution with numerical simulation when k* and De are 0 and 0.01 for different parameters in case I, which are a) stream function; (b) distribution of velocity; (c) distribution of stress; (d) dimensionless temperature.

3.1.2. Case II: The Maxwell upper-convected fluid flow in the porous medium on the horizontal surface

Like the ordinary plate, i.e., the one which is not composed of a porous medium, here for the porous medium, the validation is carried out using a similar way. The results are depicted in Fig. 5a–d for the stream function, velocity distribution, stress distribution, and dimensionless temperature, respectively. As observed, the made comparison reveals the high accuracy of the provided HPM solution in prediction.

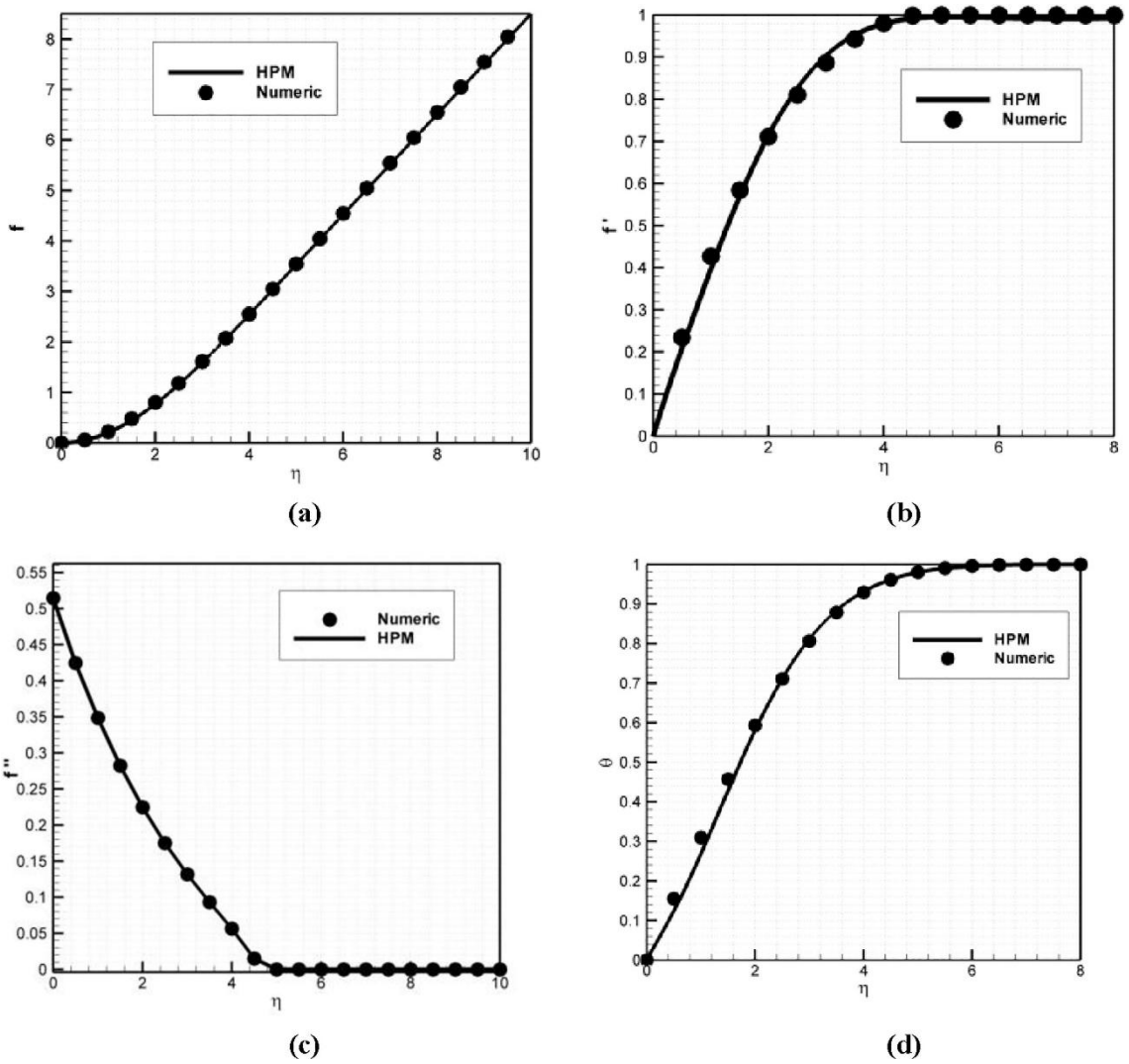

Fig. 5. Checking the prediction ability of the proposed analytical solution with numerical simulation when k* and De are 0.2 and 0.1 for different parameters in case II, which are a) stream function; (b) distribution of velocity; (c) distribution of stress; (d) dimensionless temperature.

3.2. Sensitivity analysis

By employing the validated HPM solution, the sensitivity analysis is carried out to find the impact of Deborah (De) on stream function, velocity and stress distribution. It is done for flowing the Maxwell upper-convected fluid for both the investigated material for the horizontal surface, i.e., ordinary and porous conditions.

3.2.1. Case I: The Maxwell upper-convected fluid on the horizontal surface

Fig. 6, Fig. 7, Fig. 8 present the results for this case. As shown in Fig. 6, when De goes up, initially, stream function has an upward trend. However, it then goes down, which is followed by an increase in the velocity in the direction of y.

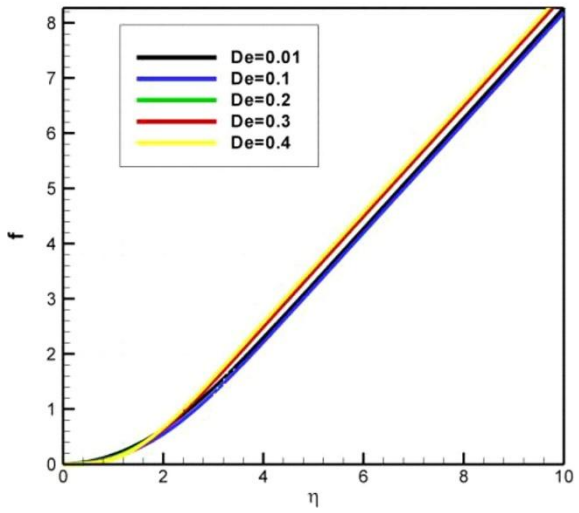

Fig. 6. The impacts of De on the stream function in case I.

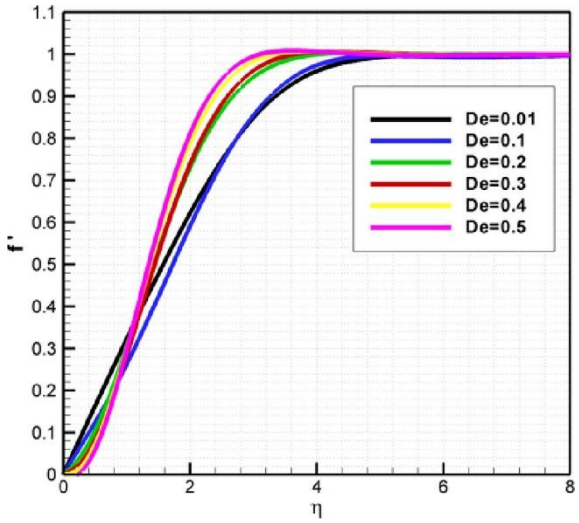

Fig. 7. The impacts of De on the velocity distribution in case I.

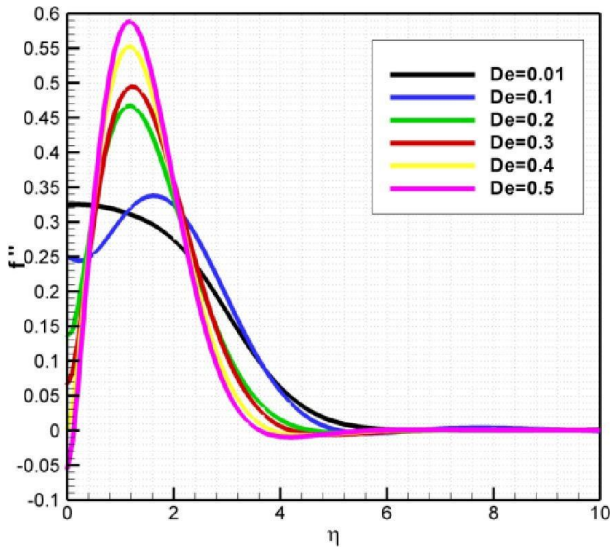

Fig. 8. The impacts of De on the stress distribution in case I.

As shown in Fig. 7, Fig. 8, the velocity within the boundary layer increases by increasing η, but the shear stress goes down. The reason is that by increasing η and not changing x, the distance from the wall becomes more, which is accompanied by getting lower effect from the wall. As a result, the shear stress has a downward trend and the velocity becomes closer to the free flow rate.

Deborah number is a dimensionless value which describes the ratio of the relaxation time (t_c) to the time scale characteristic for a test probing the reaction of the substance (t_p) [59]:

$$\mathrm{De} = \frac{t_c}{t_p} \tag{67}$$

As shown in Fig. 7, as De for the Maxwell upper-convected fluid increases, the velocity profile decreases first and then, increases rapidly, but the thickness of the hydrodynamic boundary layer goes down. In addition, according to Fig. 8, when De increases, the stress distribution first increases and next, tends to zero at the further points, but is decreasing on the plate. It is because of the fact that when De increases, the elasticity of the fluid increases, but its viscosity decreases. As a result, the stress on the plate have a downward trend. Moreover, based on Fig. 8, for De = 0.5 the stress on the plate has a negative value, which indicates that, the separation operation has occurred and the considered hypotheses for boundary layer are no longer true. Table 3 shows the skin friction coefficient for different values of De. According to Table 3, it is concluded that by increasing De, the skin friction coefficient goes down.

Table 3. Values of the skin friction coefficient for different conditions of De (when k* is 0).

De	0	0.01	0.1	0.2	0.3	0.4
f''(0)	0.3320	0.3245	0.2500	0.1347	0.0659	0.0016

In addition, Fig. 9 shows the heat distribution in the boundary layer. This figure implies that as η increases, the temperature profile, i.e., $\theta(\eta)$ increases. Moreover, when De increases, the temperature distribution goes up, but the thickness of the thermal boundary layer decreases.

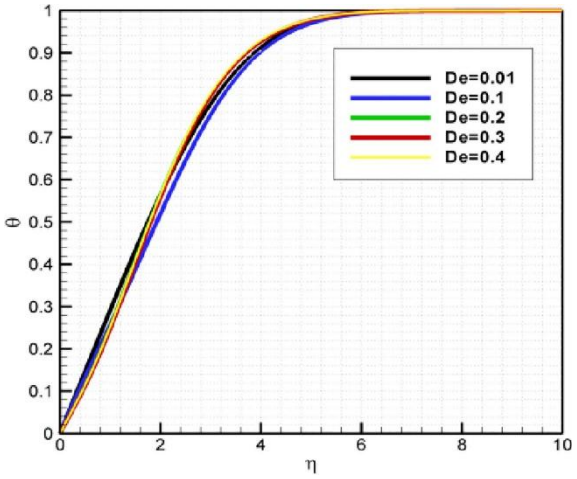

Fig. 9. Temperature profile for different values of De in case I.

Fig. 10 also illustrates the temperature gradient for different values of De. Based on Fig. 10, it is implied that as De increases, the heat gradient on the plate decreases, which means the heat transfer rate between the plate and the fluid goes down.

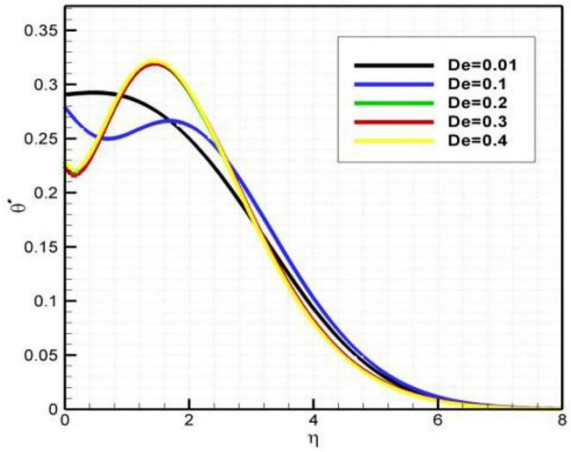

Fig. 10. Temperature gradient for different values of De in case I.

3.2.2. Case II: The Maxwell upper-convected fluid flow in the porous medium on the horizontal surface

Fig. 11 reports the results for the dimensionless stream function, while Fig. 12, Fig. 13 presents the variation trend for velocity distribution and stress distribution, respectively. Increasing De leads to a linear growth for f. Moreover, Fig. 12, Fig. 13 show that as

increases, the velocity within the boundary layer goes up, whereas the shear stress decrease. The reason is by increasing η, the influence of wall region at the same value for x goes down. Consequently, as we the shear stress declines and the velocity gets closer to the velocity of free stream.

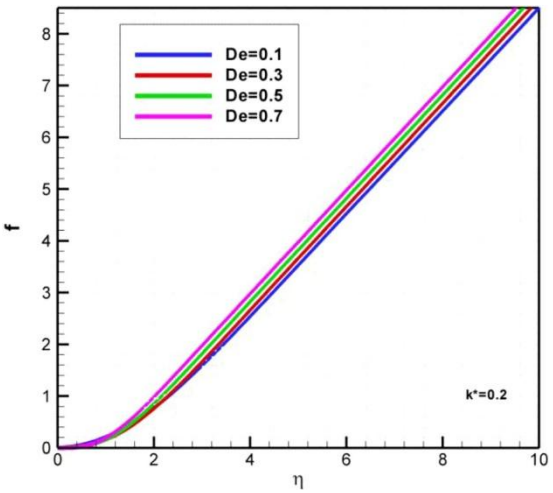

Fig. 11. The impacts of De on the stream function in case II.

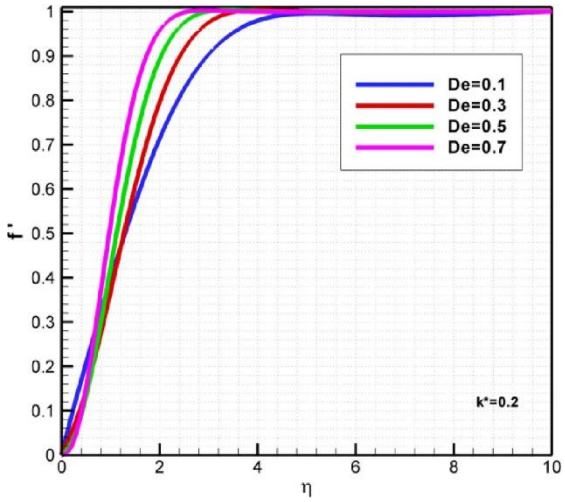

Fig. 12. The impacts of De on the velocity distribution in case II.

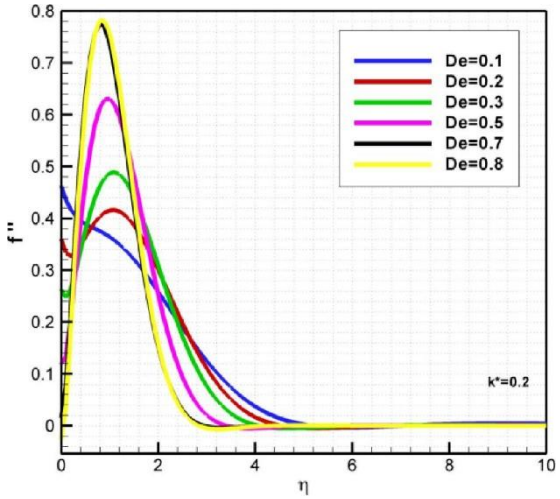

Fig. 13. The impacts of De on the stress distribution in case II.

Based on the reported results in Fig. 12, in case the porosity remains constant, De increases. Moreover, the velocity profile decreases first and then, increases rapidly. Nonetheless, the thickness of the hydrodynamic boundary layer goes down.

According to Fig. 13, by increasing De, the stress distribution increases first and tends to zero at farther points, afterwards. However, has an upward trend on the plate, so that at De = 0.8, it finds a negative value, which means in that region, the hypotheses of the boundary layer is no longer applicable. Therefore, the solution corresponds to De = 0.7. It could be interpreted by the point that the decrease in stress on the plate leads to increase De, which is accompanied by growing the elasticity of the fluid and decreasing the viscosity decreases. As a result, the stress on the plate decreases. The skin friction coefficient for different values of De is given in Table 4. According to Table 4, it is found the more De is, the lower skin friction coefficient will be.

Table 4. The values of the skin friction coefficient for different conditions of De (when K* is 0.2).

De	0	0.1	0.2	0.3	0.4	0.5	0.6	0.7
$f''(0)$	0.5060	0.4622	0.3596	0.2626	0.1885	0.1187	0.0619	0.0158

Fig. 14 also demonstrates that when η increases, the temperature profile $\theta(\eta)$ goes up. Moreover, when De increases, the temperature $\theta(\eta)$ has an upward trend, but the thickness of the thermal boundary layer declines.

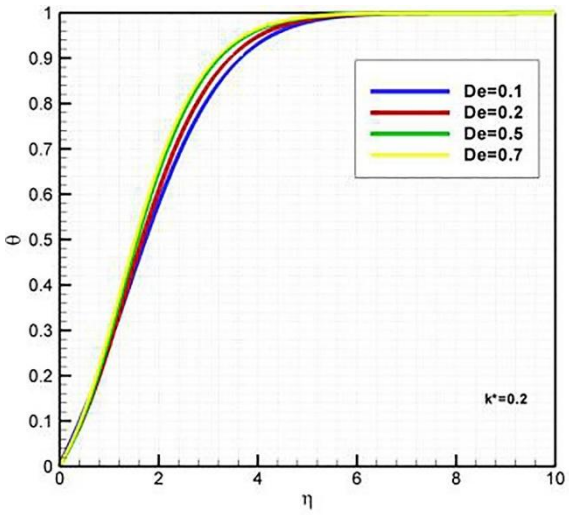

Fig. 14. Temperature profile for different values of De in case II.

Moreover, the temperature gradient for different values of De is shown in Fig. 15. According to this figure increasing De is accompanied by decreasing the heat gradient on the plate, which implies that, the heat transfer between the plate and the fluid diminishes.

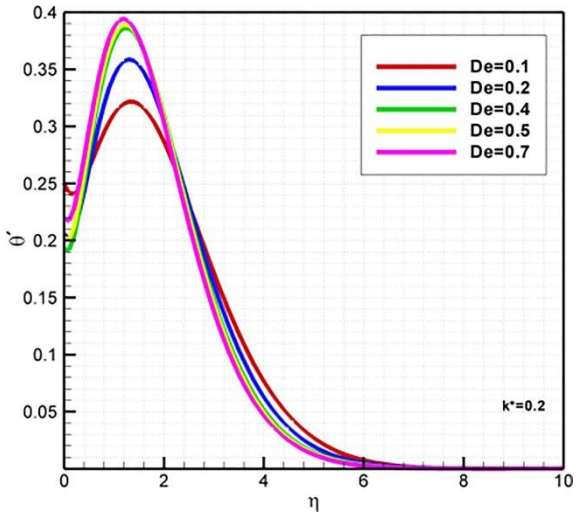

Fig. 15. Temperature gradient for different values of De in case II.

4. Conclusions

In the current work, homotopy perturbation method (HPM) was employed to find the analytical solution for flowing the Maxwell upper-convected fluid on a horizontal surface. Two possibilities for the plate material were investigated. In one of them, the plate was assumed to be not porous, whereas in another one, it was considered to be composed of a porous material. For each condition, the obtained solution was validated using the numerical simulation of the boundary value problem (BVP), and then, a sensitivity analysis was performed to find the impact of effective parameters on the solution. According to the results, the following results were obtained:

- When the penetration coefficient for the porous medium increased, the velocity profile increased, and the thickness of the hydrodynamic boundary layer declined.
- Increasing the penetration coefficient was accompanied by increasing the skin friction coefficient.
- The lower De was, the greater skin friction coefficient was observed.
- As the penetration rate of the porous medium increased, the heat transfer increased, but the increase in Deborah reduced the heat transfer.

Moreover, as the ideas for future work, the items like solving the problem for the plate with slip condition, presence of the magnetic field and thermal radiation could be suggested. In addition, the problem could be solved for movable stretch and inclined plates.

CRediT authorship contribution statement

Siamak Hoseinzadeh: Methodology, Investigation, Resources, Software, and Validation. Ali Sohani: Conceptualization, Methodology, Data curation, Project administration, Visualization, Writing - original draft, Writing - review & editing. Mohammad Hassan Shahverdian: Formal analysis, Investigation, and Resources. Amin Shirkhani: Formal analysis, Visualization, and Resources. Stephan Heyns: Resources, and Writing - review & editing.

Declaration of Competing Interest

The authors declare that they have no known competing financial interests or personal relationships that could have appeared to influence the work reported in this paper.

References

[1] V. Yerramalle, B. Premachandran, P. Talukdar, Numerical investigation of the performance of interface conditions for fluid flow through a partially filled porous channel, Therm. Sci. Eng. Progr. 20 (2020), 100628.
[2] P. B V, M. Sankar, O.D. Makinde, Optimization of thermosolutal convection in vertical porous annulus with a circular baffle, Thermal Science and Engineering Progress 20 (2020) 100735.
[3] U.S. Mahabaleshwar, K.R. Nagaraju, P.N. Vinay Kumar, M.N. Nadagouda, R. Bennacer, M.A. Sheremet, Effects of dufour and soret mechanisms on MHD mixed convective-radiative non-newtonian liquid flow and heat transfer over a porous sheet, Therm. Sci. Eng. Progr. 16 (2020), 100459.
[4] Zhuqing Luo, Hongtao Xu, Numerical simulation of heat and mass transfer through microporous media with lattice Boltzmann method, Therm. Sci. Eng. Prog. 9 (2019) 44–51.

[5] Seyyedmahan Khatami, Nader Rahbar, An analytical study of entropy generation in rectangular natural convective porous fins, Therm. Sci. Eng. Prog. 11 (2019) 142–149.
[6] Q. Wang, K. Wang, P. Li, Forced convective heat and mass transfer in a bidisperse porous parallel-plate channel with a first order reaction on the wall, Therm. Sci. Eng. Progr. 13 (2019), 100369.
[7] K.V. Srinivasan, A. Manimaran, M. Arulprakasajothi, M. Revanth, Vijay A. Arolkar, Design and development of porous regenerator for Stirling cryocooler using additive manufacturing, Therm. Sci. Eng. Progr. 11 (2019) 195–203.
[8] Hong Thai Vu, Evangelos Tsotsas, Mass and heat transport models for analysis of the drying process in porous media: a review and numerical implementation, Int. J. Chem. Eng. 2018 (2018) 1–13.
[9] K. Vafai, Handbook of Porous Media, Crc Press, 2015.
[10] I. Berre, F. Doster, E. Keilegavlen, Flow in fractured porous media: a review of conceptual models and discretization approaches, Transp. Porous Media 130 (1) (2019) 215–236.
[11] A. Sohani, M.H. Shahverdian, H. Sayyaadi, D.A. Garcia, Impact of absolute and relative humidity on the performance of mono and poly crystalline silicon photovoltaics; applying artificial neural network, J. Cleaner Prod. 276 (2020), 123016.
[12] A. Sohani, H. Sayyaadi, Employing genetic programming to find the best correlation to predict temperature of solar photovoltaic panels, Energy Convers. Manage. 224 (2020), 113291.
[13] Ali Sohani, Hoseyn Sayyaadi, Sina Hoseinpoori, Modeling and multi-objective optimization of an M-cycle cross-flow indirect evaporative cooler using the GMDH type neural network, Int. J. Refrig 69 (2016) 186–204.
[14] Ali Sohani, Hoseyn Sayyaadi, Providing an accurate method for obtaining the efficiency of a photovoltaic solar module, Renew. Energy 156 (2020) 395–406.
[15] Ashkan Javadzadegan, Mohammad Joshaghani, Abouzar Moshfegh, Omid Ali Akbari, Hamid Hassanzadeh Afrouzi, Davood Toghraie, Accurate meso-scale simulation of mixed convective heat transfer in a porous media for a vented square with hot elliptic obstacle: an LBM approach, Phys. A 537 (2020) 122439, https:// doi.org/10.1016/j.physa:2019.122439.
[16] Mohsen Sheikholeslami, Numerical simulation of magnetic nanofluid natural convection in porous media, Phys. Lett. A 381 (5) (2017) 494–503.
[17] Mohammad Hesam Toosi, Majid Siavashi, Two-phase mixture numerical simulation of natural convection of nanofluid flow in a cavity partially filled with porous media to enhance heat transfer, J. Mol. Liq. 238 (2017) 553–569.
[18] Mostafa Moghaddami, Seyedehsan Shahidi, Majid Siavashi, Entropy generation analysis of nanofluid flow in turbulent and laminar regimes, J. Comput. Theor. Nanosci. 9 (10) (2012) 1586–1595.
[19] Elsayed Abdelfatah, Maysam Pournik, Bor Jier Ben Shiau, Jeffrey Harwell, Mathematical modeling and simulation of nanoparticles transport in heterogeneous porous media, J. Nat. Gas Sci. Eng. 40 (2017) 1–16.
[20] M. Jourabian, A.A.R. Darzi, D. Toghraie, O.a. Akbari, Melting process in porous media around two hot cylinders: Numerical study using the lattice Boltzmann method, Physica A: Statistical Mechanics and its Applications 509 (2018) 316-335.
[21] Abbas Khayyer, Hitoshi Gotoh, Yuma Shimizu, Kohji Gotoh, Hosein Falahaty, Songdong Shao, Development of a projection-based SPH method for numerical wave flume with porous media of variable porosity, Coast. Eng. 140 (2018) 1–22.
[22] R. Ellahi, Sadiq M. Sait, N. Shehzad, Z. Ayaz, A hybrid investigation on numerical and analytical solutions of electro-magnetohydrodynamics flow of nanofluid through porous media with entropy generation, Int. J. Numer. Meth. Heat Fluid Flow 30 (2) (2019) 834–854.
[23]Junwei Su, Guoliang Chai, Le Wang, Weidong Cao, Zhaolin Gu, Chungang Chen, Xiao Yun Xu, Pore-scale direct numerical simulation of particle transport in porous media, Chem. Eng. Sci. 199 (2019) 613–627.

[24] P. Talebizadeh Sardari, G.S. Walker, M. Gillott, D. Grant, D. Giddings, Numerical modelling of phase change material melting process embedded in porous media: effect of heat storage size, Proceedings of the institution of mechanical engineers, Part A: journal of power and energy 234(3) (2020) 365-383.
[25] S. Nazari, R. Ellahi, M.M. Sarafraz, M.R. Safaei, A. Asgari, O.A. Akbari, Numerical study on mixed convection of a non-Newtonian nanofluid with porous media in a two lid-driven square cavity, J. Therm. Anal. Calorim. 140 (3) (2020) 1121–1145.
[26] S. Omirbekov, H. Davarzani, S. Colombano, A. Ahmadi-Senichault, Experimental and numerical upscaling of foam flow in highly permeable porous media, Adv. Water Resour. 146 (2020), 103761.
[27] M. Chen, X. Li, S. Tong, K. Mohanty, Y. Wang, W. Yang, R. Hazlett, J. Lu, Experimental investigation and numerical modeling of barium sulfate deposition in porous media, J. Petrol. Sci. Eng. 195 (2020), 107920.
[28] C. Hu, M. Sun, Z. Xie, L. Yang, Y. Song, D. Tang, J. Zhao, Numerical simulation on the forced convection heat transfer of porous medium for turbine engine heat exchanger applications, Appl. Therm. Eng. 180 (2020), 115845.
[29] E. Aminian, H. Moghadasi, H. Saffari, Magnetic field effects on forced convection flow of a hybrid nanofluid in a cylinder filled with porous media: a numerical study, J. Therm. Anal. Calorim. 141 (5) (2020) 2019–2031.
[30] N. Hosseini, Z. Bajalan, A.R. Khoei, Numerical modeling of density-driven solute transport in fractured porous media with the extended finite element method, Adv. Water Resour. 136 (2020), 103453.
[31] N. Massarotti, A. Mauro, V. Trombetta, A general numerical procedure for solidification and melting in porous media and free fluids, Int. J. Therm. Sci. 161 (2021) 106716, https://doi.org/10.1016/j.ijthermalsci.2020.106716.
[32] X.-B. Feng, Q. Liu, Y.-L. He, Numerical simulations of convection heat transfer in porous media using a cascaded lattice Boltzmann method, Int. J. Heat Mass Transf. 151 (2020), 119410.
[33] Ali Sohani, Hoseyn Sayyaadi, Hamidreza Hasani Balyani, Sina Hoseinpoori, A novel approach using predictive models for performance analysis of desiccant enhanced evaporative cooling systems, Appl. Therm. Eng. 107 (2016) 227–252.
[34] Mehdi Dehghan, Fatemeh Shakeri, Use of He's homotopy perturbation method for solving a partial differential equation arising in modeling of flow in porous media, J. Porous Media 11 (8) (2008) 765–778.
[35] Li-Mei Yan, Modified homotopy perturbation method coupled with Laplace transform for fractional heat transfer and porous media equations, Thermal Sci. 17 (5) (2013) 1409–1414.
[36] D.D. Ganji, A. Sadighi, Application of homotopy-perturbation and variational iteration methods to nonlinear heat transfer and porous media equations, J. Comput. Appl. Math. 207 (1) (2007) 24–34.
[37] Erdem Cuce, Pinar Mert Cuce, A successful application of homotopy perturbation method for efficiency and effectiveness assessment of longitudinal porous fins, Energy Convers. Manage. 93 (2015) 92–99.
[38] Behrouz Raftari, Ahmet Yildirim, The application of homotopy perturbation method for MHD flows of UCM fluids above porous stretching sheets, Comput. Math. Appl. 59 (10) (2010) 3328–3337.
[39] Ahmet Yildirim, Sefa Anil Sezer, Analytical solution of MHD stagnation-point flow in porous media by means of the homotopy perturbation method, J. Porous Media 15 (1) (2012) 83–94.
[40] Seyfolah Saedodin, Majid Shahbabaei, Thermal analysis of natural convection in porous fins with homotopy perturbation method (HPM), Arab. J. Sci. Eng. 38 (8) (2013) 2227–2231.

[41] Q. Shao, M. Fahs, A. Younes, A. Makradi, A high-accurate solution for darcy- brinkman double-diffusive convection in saturated porous media, Numer. Heat Trans. Part B Fundam. 69 (1) (2016) 26–47.
[42] Marwan Fahs, Thomas Graf, Tuong Vi Tran, Behzad Ataie-Ashtiani, Craig. T. Simmons, Anis Younes, Study of the effect of thermal dispersion on internal natural convection in porous media using Fourier series, Transp. Porous Media 131 (2) (2020) 537–568.
[43] Q. Shao, M. Fahs, A. Younes, A. Makradi, T. Mara, A new benchmark reference solution for double-diffusive convection in a heterogeneous porous medium, Numer. Heat Trans. Part B Fundam. 70 (5) (2016) 373–392.
[44] Abiola D. Obembe, M. Enamul Hossain, Kassem Mustapha, Sidqi A. Abu-Khamsin, A modified memory-based mathematical model describing fluid flow in porous media, Comput. Math. Appl. 73 (6) (2017) 1385–1402.
[45] M.R. Shirkhani, H.A. Hoshyar, I. Rahimipetroudi, H. Akhavan, D.D. Ganji, Unsteady time-dependent incompressible Newtonian fluid flow between two parallel plates by homotopy analysis method (HAM), homotopy perturbation method (HPM) and collocation method (CM), Propul. Power Res. 7 (3) (2018) 247–256.
[46] K.B. Nakshatrala, S.H.S. Joodat, R. Ballarini, Modeling flow in porous media with double porosity/permeability: mathematical model, properties, and analytical solutions, J. Appl. Mech. 85 (8) (2018).
[47] S.H.S. Joodat, K.B. Nakshatrala, R. Ballarini, Modeling flow in porous media with double porosity/permeability: a stabilized mixed formulation, error analysis, and numerical solutions, Comput. Methods Appl. Mech. Eng. 337 (2018) 632–676.
[48] S. Hoseinzadeh, P.S. Heyns, A.J. Chamkha, A. Shirkhani, Thermal analysis of porous fins enclosure with the comparison of analytical and numerical methods, J. Therm. Anal. Calorim. 138 (1) (2019) 727–735.
[49] Ali Nabizadeh, Mohammad Sharifi, Babak Aminshahidi, An analytical solution for spherical fluid flow modeling in porous media with non-uniform initial pressure considering the supercharging effect, Petroleum (2020), https://doi.org/10.1016/j.petlm.2020.10.006.
[50] T. Ghanbari Ashrafi, S. Hoseinzadeh, A. Sohani, M.H. Shahverdian, Applying Homotopy Perturbation Method to Provide an Analytical Solution for Newtonian Fluid Flow on A Porous Flat Plate (In press), Mathematical Methods in the Applied Sciences (2021), doi: 10.1002/mma.7238.
[51] J.-H. He, Homotopy perturbation technique, Comput. Methods Appl. Mech. Eng. 178 (3) (1999) 257–262.
[52] N. Anjum, J.-H. He, Higher-order homotopy perturbation method for conservative nonlinear oscillators generally and microelectromechanical systems' oscillators particularly, Int. J. Mod. Phys. B 2050313 (2020).
[53] N. Anjum, J.-H. He, Two Modifications of the Homotopy Perturbation Method for Nonlinear Oscillators, J. Appl. Comput. Mech. (2020).
[54] J.-H. He, Y.O. El-Dib, Homotopy perturbation method for Fangzhu oscillator, J. Math. Chem. 58 (10) (2020) 2245–2253.
[55] J.H. He, Y.O. El-Dib, The reducing rank method to solve third-order Duffing equation with the homotopy perturbation, Numer. Methods Partial Differen. Equat. (2020).
[56] S. Noeiaghdam, A. Dreglea, J. He, Z. Avazzadeh, M. Suleman, M.A. Fariborzi Araghi, D.N. Sidorov, N. Sidorov, Error Estimation of the Homotopy Perturbation Method to Solve Second Kind Volterra Integral Equations with Piecewise Smooth Kernels: Application of the CADNA Library, Symmetry 12(10) (2020) 1730.
[57] S. Saleem, M. Awais, S. Nadeem, N. Sandeep, M.T. Mustafa, Theoretical analysis of upper-convected Maxwell fluid flow with Cattaneo-Christov heat flux model, Chin. J. Phys. 55 (4) (2017) 1615–1625.

[58] Maplesft, The online help about dsolve/numeric/BVP <https://www.maplesoft.com/support/help/Maple/view.aspx?path=dsolve/numeric/BVP>; Accessed on December 31, 2020., (2020).
[59] R.J. Poole, The deborah and weissenberg numbers, Rheol. Bull 53 (2) (2012) 32–39.